

The coherent structure of the energy cascade in isotropic turbulence

Danah Park¹† and Adrián Lozano-Durán

¹Mechanical Engineering Department, Stanford University, Stanford, CA 94305, USA

²Department of Aeronautics and Astronautics, Massachusetts Institute of Technology, Cambridge, MA, 02139, USA

(Received xx; revised xx; accepted xx)

The energy cascade, i.e. the transfer of kinetic energy from large-scale to small-scale flow motions, has been the cornerstone of turbulence theories and models since the 1940s. However, understanding the spatial organization of the energy transfer has remained elusive. In this study, we utilize numerical data of isotropic turbulence to investigate the three-dimensional spatial structure of the energy cascade. Specifically, we focus on analyzing the averaged flow patterns associated with intense energy transfer events in the inertial range. Our findings indicate that forward energy-transfer events are predominantly confined in the high strain-rate region created between two distinct zones of elevated enstrophy. On average, these zones manifest in the form of two hairpin-like shapes with opposing orientations. The mean velocity field associated with the energy transfer exhibits a saddle point topology when observed in the frame of reference local to the event. The analysis also suggests that the primary driving mechanism for energy transfer involves strain-rate self-amplification among local scales, followed closely by non-local interactions that promote interscale vortex stretching and strain self-amplification.

Key words:

1. Introduction

Turbulence exhibits a wide range of flow scales, whose non-linear interactions still challenge our intellectual ability to understand even the simplest flows. These interactions are responsible for the cascading of kinetic energy from large eddies to the smallest eddies, where the energy is finally dissipated (e.g. Richardson 1922; Obukhov 1941; Kolmogorov 1941). Given the ubiquity of turbulence, a deeper understanding of the energy transfer among flow scales would enable significant progress to be made across various fields ranging from combustion (e.g. Veynante & Vervisch 2002), meteorology (e.g. Bodenschatz 2015), and astrophysics (e.g. Young & Read 2017) to engineering applications of external aerodynamics and hydrodynamics (e.g. Sirovich & Karlsson 1997; Hof *et al.* 2010; Marusic *et al.* 2010; Kühnen *et al.* 2018).

The phenomenological description of the turbulent cascade in terms of interactions among eddies at different scales was first proposed by Richardson (1920) and later by Obukhov (1941). Since then, substantial efforts have been directed toward the characterization of inter-scale kinetic energy transfer. The statistical description of the transfer of energy from large to small scales was introduced in the classical paper by Kolmogorov

† Email address for correspondence: danah12@stanford.edu

(1941). Since then, a large body of research has been devoted to addressing two outstanding questions about the energy cascade: 1) Is the transfer of kinetic energy from large to small scales local in scale? and 2) What are the physical mechanisms driving the transfer of energy among scales? Here, we pose a third question: 3) What are the characteristic flow patterns surrounding regions of intense energy transfer? The three questions above are interconnected, and we anticipate that addressing question 3) will shed some light on question 2).

There is general agreement from the community that the answer to the first question is yes. The net transfer of energy from large to small scales is mainly accomplished by interactions among flow motions of similar size. The conclusion is supported by evidence from diverse approaches, such as scaling analysis (Zhou 1993*a,b*; Eyink 1995; Aoyama *et al.* 2005; Eyink 2005; Mininni *et al.* 2006, 2008; Aluie & Eyink 2009; Eyink & Aluie 2009), triadic interactions in Fourier space (Domaradzki & Rogallo 1990; Domaradzki *et al.* 2009), and time correlations (Cardesa *et al.* 2015, 2017), to name a few.

The degree of consensus is lower regarding the second question. Several theories have been proposed to describe the physical mechanism(s) that enable the transfer of energy from larger to smaller scales throughout the inertial range. One of the first mechanisms proposed is based on the concept of vortex stretching. In this scenario, vorticity is stretched by the strain-rate either at the same scale or at a larger scale (Taylor & Green 1937; Taylor 1938; Tennekes *et al.* 1972; Davidson *et al.* 2008; Hamlington *et al.* 2008; Leung *et al.* 2012; Lozano-Durán *et al.* 2016; Doan *et al.* 2018). Some authors have further proposed that the mechanistic details of the process can be explained by successive reconnections of anti-parallel vortex tubes (Melander & Hussain 1988; Hussain & Duraisamy 2011; Goto *et al.* 2017; Yao & Hussain 2020), vortex reconnection of two long, straight anti-parallel vortex tubes with localized bumps (Kerr 2013), and the presence of helical instabilities in characteristic of vortex rings (Brenner *et al.* 2016; McKeown *et al.* 2018). These viewpoints, while not dynamically equivalent, are still compatible with the vortex-stretching driven energy cascade.

The main competing theory to the vortex stretching mechanism is the self-amplification of the rate-of-strain either by same-scale interactions or by the amplification from larger scale strain-rate (e.g. Tsinober 2009; Paul *et al.* 2017; Sagaut & Cambon 2008; Carbone & Bragg 2020; Vela-Martín & Jiménez 2021). In both scenarios, the strain-rate self-amplification stands as the key contributor to the transfer of energy among scales, whereas vortex stretching is merely the effect (rather than the cause) of the energy cascade. Given the kinematic relationship between vortex stretching and strain-rate self-amplification (Betchov 1956; Capocci *et al.* 2023), some authors have argued that both mechanisms play a relevant role in the dynamics of the energy cascade (Johnson 2020, 2021).

The studies above have helped advance our understanding of the physics of the energy cascade; however, less is known about flow patterns associated with the cascading process. With the advent of novel flow identification techniques (e.g. del Álamo *et al.* 2004; Lozano-Durán *et al.* 2012; Lozano-Durán & Jiménez 2014; Dong *et al.* 2017, 2020), the three-dimensional characterization of turbulent structures is now achievable to complete the picture. In this work, we shed light on the characteristic flow patterns associated with the energy cascade by investigating the spatial three-dimensional structure of the flow conditioned to intense energy transfer events. The work is organized as follows. The method is presented in §2, where we introduce the numerical dataset, filtering procedure, structure identification, and conditional flow field methodology. The results concerning the dominant flow patterns associated with the energy transfer are discussed in §3 and conclusions are offered in §4.

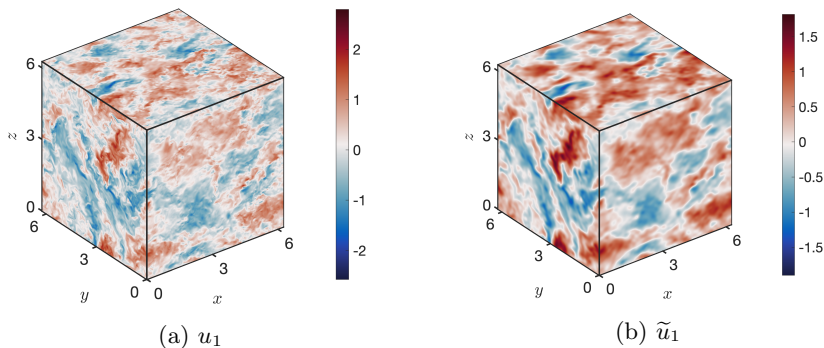


Figure 1: Instantaneous velocity field for (a) u_1 and (b) \tilde{u}_1 . The velocity is normalized by $\sqrt{\langle u_i u_i \rangle}$ in panel (a) and by $\sqrt{\langle \tilde{u}_i \tilde{u}_i \rangle}$ in panel (b), where $\langle \cdot \rangle$ denotes average over homogeneous directions and time.

2. Methods

2.1. Numerical dataset and filtering procedure

We use direct numerical simulations of isotropic turbulence from Cardesa *et al.* (2015). The numerical setup corresponds to isotropically forced turbulence within a triply periodic domain at Reynolds numbers $\text{Re}_\lambda = 146$ and $\text{Re}_\lambda = 236$, where Re_λ represents the Reynolds number based on the Taylor-microscale λ . The reader is referred to Cardesa *et al.* (2015) for additional details about the numerical setup. In our analysis, similar conclusions were drawn for both Reynolds numbers and the findings pertaining to $\text{Re}_\lambda = 146$ are omitted here for brevity.

To investigate the structure of the energy transfer, the velocity field is decomposed into large and small scales using a low-pass Gaussian filter such that $u_i = \tilde{u}_i + u'_i$, where u_i represents the i -th component of the instantaneous velocity, \tilde{u}_i is the filtered velocity, and u'_i corresponds to the remaining fluctuating velocity component. The filter kernel is isotropic and given in Fourier space by $\hat{G}(\mathbf{k}) = \exp[-(r|\mathbf{k}|)^2/24]$, where \mathbf{k} denotes the wavevector, and r is the filter width. The filter width selected is $r = 30\eta$, where η is the Kolmogorov length-scale. The value was chosen to lie within the inertial range of the turbulence cascade (Cardesa *et al.* 2015). It was assessed that the conclusions shown below remain consistent when the analysis is repeated with the filter width $r = 60\eta$. Figure 1 illustrates one instant for both the unfiltered and filtered velocity for $r = 30\eta$.

2.2. Identification of intense energy transfer events

The kinetic energy equation for the filtered velocity field is

$$\frac{D}{Dt} \left(\frac{1}{2} \tilde{u}_i \tilde{u}_i \right) = - \frac{\partial}{\partial x_j} \left(\tilde{u}_j \tilde{p} + \tilde{u}_i \tau_{ij} - 2\nu \tilde{u}_i \tilde{S}_{ij} \right) - 2\nu \tilde{S}_{ij} \tilde{S}_{ij} - \Pi + \tilde{u}_i \tilde{f}_i, \quad (2.1)$$

where repeated indices imply summation, $D/Dt = \partial/\partial t + \tilde{u}_j \partial/\partial x_j$ is the material derivative, ν is the kinematic viscosity, $\tilde{S}_{ij} = (\partial \tilde{u}_i / \partial x_j + \partial \tilde{u}_j / \partial x_i) / 2$ is the strain-rate tensor for the filtered velocity, and \tilde{f}_i is the forcing term. The first and second terms on the right-hand side of Eq. (2.1) represent the spatial flux of the kinetic energy and dissipation of the energy, respectively. The term $\Pi = -(\tilde{u}_i \tilde{u}_j - \tilde{u}_i \tilde{u}_j) \tilde{S}_{ij}$ is the inter-scale kinetic energy transfer, which is the quantity of interest here. A positive value of Π signifies the transfer of kinetic energy from scales above the filter cut-off to smaller scales (forward

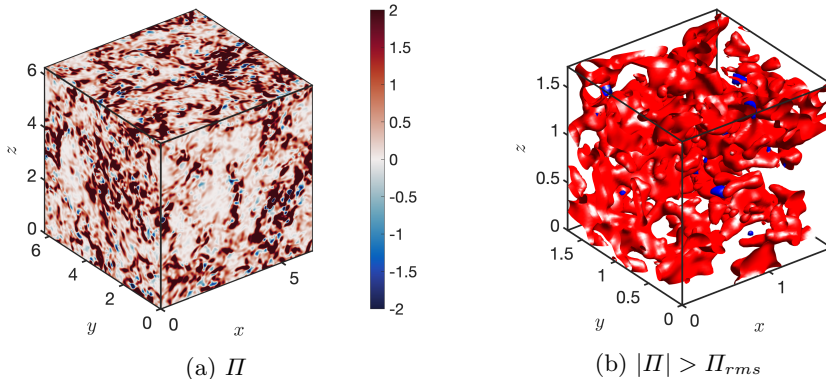


Figure 2: Instantaneous inter-scale kinetic energy transfer. (a) Π and (b) regions with $\Pi > \Pi_{rms}$ (red) and $\Pi < -\Pi_{rms}$ (blue).

cascade). Conversely, a negative value of Π indicates the transfer of kinetic energy from sub-filtered flow motions to scales above the filter cut-off (backward cascade).

The instantaneous inter-scale kinetic energy transfer at one instance is visualized in Figure 2(a). Here, our primary focus is directed toward analyzing the coherent structure of the flow in the vicinity of intense forward cascade events. Regions of strong positive Π are isolated by thresholding the field with the parameter $\alpha > 0$, such that $\Pi > \alpha \Pi_{rms}$, where Π_{rms} represents the standard deviation of Π over all the dataset. The value of $\alpha = 1$ is selected following the work of [Dong *et al.* \(2020\)](#). Then, individual three-dimensional Π -structures are defined as contiguous regions in space satisfying $\Pi > \Pi_{rms}$. These structures will be utilized as markers to conditionally average the flow. It is worth remarking that Π -structures occupy less than 20% of the total fluid volume but contribute to 70% of the total kinetic energy transfer. Figure 2(b) visualizes the regions associated with forward (red, $\Pi > \Pi_{rms}$) and backward (blue, $\Pi < -\Pi_{rms}$) intense cascade events for a given snapshot. In general, Π -structures exhibit complex shapes but often resemble an elongated ellipsoid with arbitrary orientation. Forward cascade events dominate over their backward counterparts, as clearly appreciated in Figure 2(b), consistent with previous results reported in the literature (e.g. [Piomelli *et al.* 1991](#); [Borue & Orszag 1998](#); [Cerutti & Meneveau 1998](#)).

2.3. Conditional-averaged flow fields

Figure 3 contains an schematic of the conditional average procedure. This process involves three steps, depicted in the figure from left to right: (i) identification of the Π -structures, (ii) alignment of the local frame of reference, and (iii) computation of the conditional-averaged flow field. Each step is discussed below:

(i) Identification of the Π -structures. Individual Π -structures are identified following the thresholding approached discussed in §2.2. Examples of three individual Π -structures are shown in Figure 3. A characteristic length-scale is assigned to each Π -structure by utilizing the diagonal of the local bounding box in a local frame of reference, as discussed in the next step. Our interest lies in studying structures that are of similar size as the filter width. Π -structures larger than half the length of the domain size are excluded from the analysis. Structures smaller than the filter width are also disregarded. A total number of 48 snapshots are used to extract Π -structures. Each snapshot typically contains between 700 to 800 valid Π -structures, resulting in roughly 37,000 objects that are considered for the analysis.

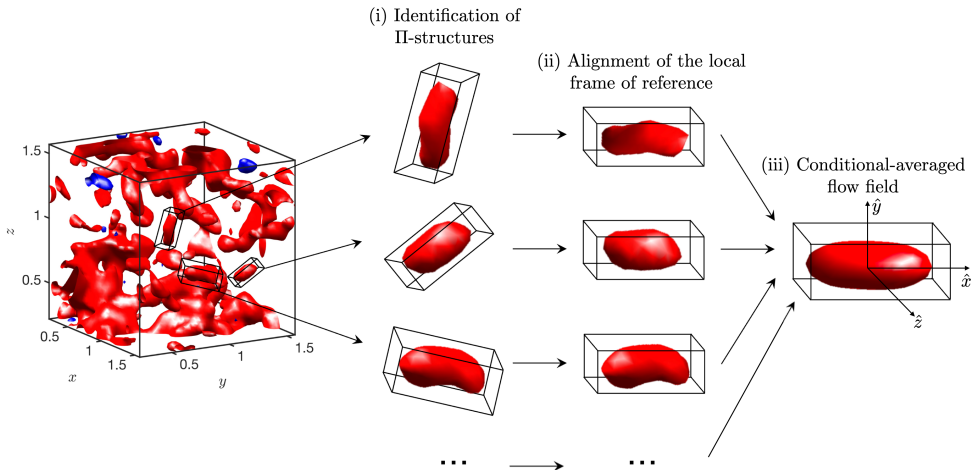


Figure 3: Schematic of the conditional average procedure.

(ii) Alignment of the local frame of reference. Each individual Π -structure is assigned a local frame of reference. The origin of the frame of reference is positioned at the center of gravity of the Π -structure. The directions of the axes are aligned with the principal axes of inertia of the object, determined by the eigenvectors of the moment of inertia tensor relative to the center of mass. A rotation matrix is constructed from these eigenvectors and used to rotate the flow field surrounding each structure. Figure 3 shows the rotated bounding boxes for three different Π -structures. Note that the coordinate system aligned with the principal axes of inertia does not inherently establish the positive or negative direction of the axes. To resolve this ambiguity, we determine the direction of the axes such that the highest enstrophy ($\tilde{\omega}_i \tilde{\omega}_i$), averaged over the bounding box of the structure is located in the first quadrant.

(iii) Computation of the conditional-averaged flow field. Conditional-averaged quantities are computed by ensemble averaging over the Π -structures in the local frame of reference. Prior to performing the average, the spatial coordinates of the local frame of reference attached to each individual structure are re-scaled based on the diagonal of the rotated bounding box of the Π -structure. Then, the conditional average for the quantity ϕ , denoted by $\{\phi\}$, is calculated as

$$\{\phi\}(\hat{\mathbf{x}}) = \sum_{n=1}^N \frac{\phi(\mathbf{x}_n + d_n \hat{\mathbf{x}})}{N}, \quad (2.2)$$

where $n = 1, \dots, N$ is the label for each Π -structure (with N the total number of samples), \mathbf{x}_n is the center of gravity of the n -th Π -structure, d_n is the diagonal length of bounding box of the n -th Π -structure, and $\hat{\mathbf{x}}$ is the space coordinate relative to the local frame of reference, re-scaled by the diagonal length.

3. Results

3.1. Conditional-averaged flow surrounding intense cascade events

Prior to analyzing the conditional-averaged flow, we offer examples of the instantaneous field surrounding the Π -structures. Figure 4 portrays two representative cases of intense

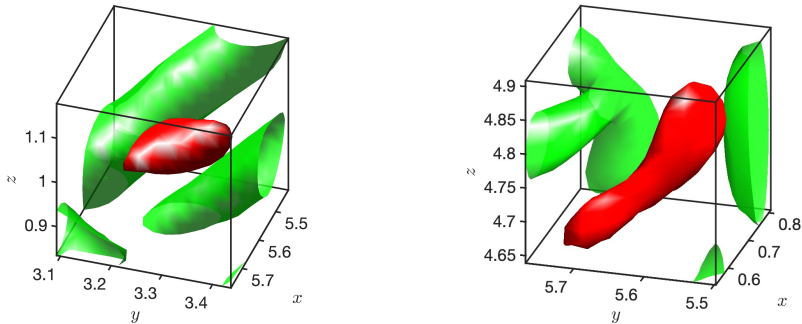


Figure 4: Instantaneous fields near intense cascade events: iso-surfaces of high transfer regions $\Pi > \Pi_{rms}$ (red) and high enstrophy regions at $0.025 \times \max(\tilde{\omega}_i \tilde{\omega}_i)$ (green).

energy transfer events, showing regions where $\Pi > \Pi_{rms}$ (colored in red) surrounded by areas of high enstrophy $\tilde{\omega}_i \tilde{\omega}_i$ (colored in green). In these specific examples, multiple vortex tubes are closely situated near the Π -structure, albeit without overlapping in space. Similar instances were consistently observed consisting of regions of intense Π surrounded by non-overlapping regions of intense $\tilde{\omega}_i \tilde{\omega}_i$. Although certain Π -structures did overlap with the vortex tubes, such occurrences were less frequent.

The dominant statistical patterns surrounding intense energy transfer events are revealed in Figure 5 and Figure 6. Figure 5 displays the streamlines of the conditional-averaged velocity field ($\{u\}, \{v\}, \{w\}$) in the vicinity of the Π -structures after subtracting the mean velocity at the origin of the Π -structure. The region of intense energy transfer is represented by a red iso-surface, corresponding to 0.6 of the maximum probability of finding a point belonging to the Π -structure (i.e., $P(\Pi > \Pi_{rms}) = 0.6$). The emerging averaged shape is an elongated ellipsoid, consistent with the patterns observed in the instantaneous field objects. Figure 5 also provides a visualization of the nearby velocity field pattern at different planes. Notably, the flow exhibits a saddle point topology centered at the origin of the Π -structure, which is a characteristic signature of strain-dominated regions. Similar patterns have previously been reported in the context of sweep and ejection pairs in homogeneous shear turbulence (Dong *et al.* 2020) and wall-bounded turbulence (Natrajan & Christensen 2006; Hong *et al.* 2012). However, the results presented here specifically pertain to the inertial range of isotropic turbulence.

The enstrophy pattern ($\{\tilde{\omega}_i\}\{\tilde{\omega}_i\}$) surrounding intense energy transfer events is visualized in Figure 6. The red region once again represents the 0.6 probability iso-surface for locating a point belonging to a Π -structure. The iso-surfaces of the enstrophy field are set at 50% of the maximum value. To facilitate the visualization of enstrophy, the regions for $\hat{z} > 0$ and $\hat{z} < 0$ are colored in yellow and blue, respectively. Two prominent patterns emerge, indicating that the energy cascade occurs between two distinct regions of intense enstrophy. These regions manifest as hairpin-like shapes with opposing orientations that do not overlap with the region where the energy transfer reaches its maximum. It is important to note that the hairpin-like structure identified does not imply that instantaneous vortices are shaped in that manner. Rather, it signifies that the irregular arrays of vortices tend to be preferentially located in those regions. These findings remain consistent across different Reynolds numbers and for the filter width $r = 60\eta$.

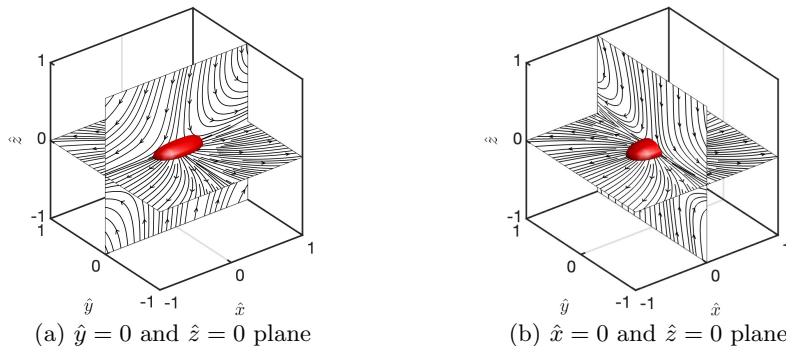


Figure 5: Conditional-averaged shape of transfer object and nearby averaged velocity streamlines: 0.6 of maximum probability of finding Π object with mean streamlines at (a) $\hat{y} = 0$ and $\hat{z} = 0$ plane and (b) $\hat{x} = 0$ and $\hat{z} = 0$ plane.

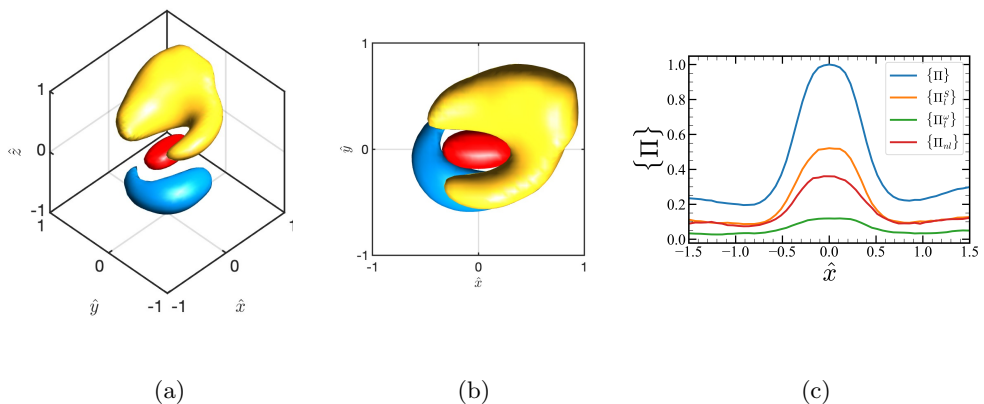


Figure 6: Iso-surface of the probability of finding a point belonging to a Π -structure equal to 0.6 (red) and enstrophy $\{\tilde{\omega}_i\}^2$ at $0.5 \times \max(\{\tilde{\omega}_i\}^2)$ at $\hat{z} > 0$ (yellow) and $\hat{z} < 0$ (blue) is shown in isometric view (a) and \hat{x} - \hat{y} projection (b). (c) Conditional-average of different energy cascade mechanism around high energy transfer events. The solid line represents $\{\Pi\}$ (blue), $\{\Pi_l^S\}$ (orange), $\{\Pi_l^\omega\}$ (green), and $\{\Pi_{nl}\}$ (red) normalized with the maximum of $\{\Pi\}$.

3.2. Mechanisms responsible for the energy transfer

To gain further insight into the underlying mechanisms driving the energy cascade, we investigate the contributions of the vortex stretching and strain-rate self-amplification in the vicinity of intense energy transfer events. The different mechanisms are quantified following the decomposing of Π proposed by Johnson (2020),

$$\Pi = \Pi_l^S + \Pi_l^\omega + \Pi_{nl}, \quad (3.1)$$

$$\Pi_l^S = -\frac{r^2}{12} \tilde{S}_{ij} \tilde{S}_{jk} \tilde{S}_{ki}, \quad \Pi_l^\omega = \frac{r^2}{48} \tilde{\omega}_i \tilde{\omega}_j \tilde{S}_{ij}, \quad (3.2)$$

$$\Pi_{nl} = \tilde{S}_{ij} \int_0^{r^2} \left(\frac{\overline{A_{ik}^{|\cdot|}} \overline{A_{jk}^{|\cdot|}}^{\sqrt{r^2-l}}}{\overline{A_{ik}^{|\cdot|}} \overline{A_{jk}^{|\cdot|}}^{\sqrt{r^2-l}}} - \frac{\overline{A_{ik}^{|\cdot|}}^{\sqrt{r^2-l}} \overline{A_{jk}^{|\cdot|}}}{\overline{A_{ik}^{|\cdot|}} \overline{A_{jk}^{|\cdot|}}^{\sqrt{r^2-l}}} \right) dl, \quad (3.3)$$

where $\overline{(\cdot)}^{\sqrt{l}}$ denotes a low-pass Gaussian filter at scale \sqrt{l} such that $\overline{(\cdot)}^r = \widetilde{(\cdot)}$, and $A_{ij} = \partial u_i / \partial x_j$ is the velocity gradient tensor. The terms Π_l^S and Π_l^ω are the energy transfer due to local interactions of \widetilde{S}_{ij} with the local strain-rate \widetilde{S}_{ij} and local vorticity $\widetilde{\omega}_i$, respectively. The term Π_{nl} is the energy transfer due to non-local (yet close in scale) interactions of \widetilde{S}_{ij} with the subfilter-scale rate-of-strain and vorticity.

Figure 6(c) shows the conditional-averaged values for the total energy transfer ($\{\Pi\}$) and its individual terms ($\{\Pi_l^S\}$, $\{\Pi_l^\omega\}$, and $\{\Pi_{nl}\}$), plotted along the \hat{x} coordinate. The results reveal that 50% of the energy transfer is primarily attributed to local strain-rate self-amplification ($\{\Pi_l^S\}$), while 40% arises from nonlocal interactions ($\{\Pi_{nl}\}$). The contribution of local vortex stretching ($\{\Pi_l^\omega\}$) accounts for less than 10% of the overall energy transfer.

4. Conclusions

We have studied the three-dimensional structure of the flow surrounding regions of intense kinetic energy transfer in the inertial range of isotropic turbulence. To that end, the flow velocity was low-passed filtered using a Gaussian filter and the characteristic flow patterns surrounding intense energy transfer events were obtained by conditionally averaging the flow after proper translation, rotation, and re-scaling of the frame of reference. Our findings have revealed that forward intense energy-transfer events are consistently confined in the high strain-rate region located between two distinct zones of elevated enstrophy resembling hairpin-like shapes. In that region, the local velocity field associated with the energy transfer exhibits a saddle point topology characteristic of strain-dominated regions. Our analysis also highlights that the primary mechanisms driving the transfer of energy in these regions are the strain self-amplification at local scales, followed by non-local interactions that facilitate interscale vortex stretching and strain self-amplification.

Declaration of interests

The authors report no conflict of interest.

REFERENCES

- DEL ÁLAMO, J. C., JIMÉNEZ, J., ZANDONADE, P. & MOSER, R. D. 2004 Self-similar vortex clusters in the turbulent logarithmic region. *J. Fluid Mech.* **561**, 329–358.
- ALUIE, HUSSEIN & EYINK, GREGORY L 2009 Localness of energy cascade in hydrodynamic turbulence. ii. sharp spectral filter. *Phys. Fluids* **21** (11), 115108.
- AOYAMA, TOMOHIRO, ISHIHARA, TAKASHI, KANEDA, YUKIO, YOKOKAWA, MITSUO, ITAKURA, KEN'ICHI & UNO, ATSUYA 2005 Statistics of energy transfer in high-resolution direct numerical simulation of turbulence in a periodic box. *J. Phys. Soc. Japan* **74** (12), 3202–3212.
- BETCHOV, R 1956 An inequality concerning the production of vorticity in isotropic turbulence. *J. Fluid Mech.* **1** (5), 497–504.
- BODENSCHATZ, EBERHARD 2015 Clouds resolved. *Science* **350** (6256), 40–41.
- BORUE, VADIM & ORSZAG, STEVEN A 1998 Local energy flux and subgrid-scale statistics in three-dimensional turbulence. *J. Fluid Mech.* **366**, 1–31.
- BRENNER, MICHAEL P, HORMOZ, SAHAND & PUMIR, ALAIN 2016 Potential singularity mechanism for the euler equations. *Phys. Rev. Fluids* **1** (8), 084503.
- CAPOCCI, DAMIANO, JOHNSON, PERRY L., OUGHTON, SEAN, BIFERALE, LUCA & LINKMANN, MORITZ 2023 New exact betchov-like relation for the helicity flux in homogeneous turbulence. *J. Fluid Mech.* **963**, R1.

- CARBONE, MAURIZIO & BRAGG, ANDREW D 2020 Is vortex stretching the main cause of the turbulent energy cascade? *J. Fluid Mech.* **883**, R2.
- CARDESA, JOSÉ I, VELA-MARTÍN, ALBERTO, DONG, SIWEI & JIMÉNEZ, JAVIER 2015 The temporal evolution of the energy flux across scales in homogeneous turbulence. *Phys. Fluids* **27** (11), 111702.
- CARDESA, J. I., VELA-MARTÍN, A. & JIMÉNEZ, J. 2017 The turbulent cascade in five dimensions. *Science* **357** (6353), 782–784.
- CERUTTI, STEFANO & MENEVEAU, CHARLES 1998 Intermittency and relative scaling of subgrid-scale energy dissipation in isotropic turbulence. *Physics of Fluids* **10** (4), 928–937.
- DAVIDSON, PA, MORISHITA, K & KANEDA, Y 2008 On the generation and flux of enstrophy in isotropic turbulence. *J. Turb.* (9), N42.
- DOAN, NAK, SWAMINATHAN, N, DAVIDSON, PA & TANAHASHI, M 2018 Scale locality of the energy cascade using real space quantities. *Phys. Rev. Fluids* **3** (8), 084601.
- DOMARADZKI, J ANDRZEJ & ROGALLO, ROBERT S 1990 Local energy transfer and nonlocal interactions in homogeneous, isotropic turbulence. *Phys. Fluids* **2** (3), 413–426.
- DOMARADZKI, J ANDRZEJ, TEACA, BOGDAN & CARATI, DANIELE 2009 Locality properties of the energy flux in turbulence. *Phys. Fluids* **21** (2), 025106.
- DONG, SIWEI, HUANG, YONGXIANG, YUAN, XIANXU & LOZANO-DURÁN, ADRIÁN 2020 The coherent structure of the kinetic energy transfer in shear turbulence. *J. Fluid Mech.* **892**.
- DONG, S., LOZANO-DURÁN, A., SEKIMOTO, A. & JIMÉNEZ, J. 2017 Coherent structures in statistically stationary homogeneous shear turbulence. *J. Fluid Mech.* **816**, 167–208.
- EYINK, GREGORY L 1995 Local energy flux and the refined similarity hypothesis. *J. Stat. Phys.* **78**, 335–351.
- EYINK, GREGORY L 2005 Locality of turbulent cascades. *Phys. D: Nonlinear Phenomena* **207** (1–2), 91–116.
- EYINK, GREGORY L & ALUIE, HUSSEIN 2009 Localness of energy cascade in hydrodynamic turbulence. i. smooth coarse graining. *Phys. Fluids* **21** (11), 115107.
- GOTO, SUSUMU, SAITO, YUTA & KAWAHARA, GENTA 2017 Hierarchy of antiparallel vortex tubes in spatially periodic turbulence at high reynolds numbers. *Phys. Rev. Fluids* **2**, 064603.
- HAMLINGTON, PETER E, SCHUMACHER, JÖRG & DAHM, WERNER JA 2008 Local and nonlocal strain rate fields and vorticity alignment in turbulent flows. *Phys. Rev. E* **77** (2), 026303.
- HOF, BJÖRN, DE LOZAR, ALBERTO, AVILA, MARC, TU, XIAOYUN & SCHNEIDER, TOBIAS M. 2010 Eliminating turbulence in spatially intermittent flows. *Science* **327** (5972), 1491–1494.
- HONG, J., KATZ, J., MENEVEAU, C. & SCHULTZ, M. P. 2012 Coherent structures and associated subgrid-scale energy transfer in a rough-wall turbulent channel flow. *J. Fluid Mech.* **712**, 92–128.
- HUSSAIN, FAZLE & DURAISAMY, KARTHIK 2011 Mechanics of viscous vortex reconnection. *Phys. Fluids* **23** (2), 021701.
- JOHNSON, PERRY L 2020 Energy transfer from large to small scales in turbulence by multiscale nonlinear strain and vorticity interactions. *Phys. Rev. Lett.* **124** (10), 104501.
- JOHNSON, PERRY L 2021 On the role of vorticity stretching and strain self-amplification in the turbulence energy cascade. *J. Fluid Mech.* **922**, A3.
- KERR, ROBERT M 2013 Swirling, turbulent vortex rings formed from a chain reaction of reconnection events. *Phys. Fluids* **25** (6), 065101.
- KOLMOGOROV, A. N. 1941 The Local Structure of Turbulence in Incompressible Viscous Fluid for Very Large Reynolds' Numbers. In *Dokl. Akad. Nauk SSSR*, , vol. 30, pp. 301–305.
- KÜHNEN, JAKOB, SONG, BAOFANG, SCARSELLI, DAVIDE, BUDANUR, NAZMI BURAK, RIEDL, MICHAEL, WILLIS, ASHLEY P., AVILA, MARC & HOF, BJÖRN 2018 Destabilizing turbulence in pipe flow. *Nat. Phys.* **14** (4), 386–390.
- LEUNG, T, SWAMINATHAN, N & DAVIDSON, PA 2012 Geometry and interaction of structures in homogeneous isotropic turbulence. *J. Fluid Mech.* **710**, 453–481.
- LOZANO-DURÁN, A., FLORES, O. & JIMÉNEZ, J. 2012 The three-dimensional structure of momentum transfer in turbulent channels. *J. Fluid Mech.* **694**, 100–130.
- LOZANO-DURÁN, A, HOLZNER, M & JIMÉNEZ, J 2016 Multiscale analysis of the topological

- invariants in the logarithmic region of turbulent channels at a friction reynolds number of 932. *J. Fluid Mech.* **803**, 356–394.
- LOZANO-DURÁN, A. & JIMÉNEZ, J. 2014 Time-resolved evolution of coherent structures in turbulent channels: characterization of eddies and cascades. *J. Fluid. Mech.* **759**, 432–471.
- MARUSIC, I., MATHIS, R. & HUTCHINS, N. 2010 Predictive model for wall-bounded turbulent flow. *Science* **329** (5988), 193–196.
- MCKEOWN, RYAN, OSTILLA-MÓNICO, RODOLFO, PUMIR, ALAIN, BRENNER, MICHAEL P & RUBINSTEIN, SHMUEL M 2018 Cascade leading to the emergence of small structures in vortex ring collisions. *Phys. Rev. Fluids* **3** (12), 124702.
- MELANDER, MOGENS V & HUSSAIN, FAZLE 1988 Cut-and-connect of two antiparallel vortex tubes. *Stanford Univ., Studying Turbulence Using Numerical Simulation Databases, 2. Proc. 1988 Summer Program* .
- MININNI, PD, ALEXAKIS, A & POUQUET, ANNICK 2006 Large-scale flow effects, energy transfer, and self-similarity on turbulence. *Phys. Rev. E* **74** (1), 016303.
- MININNI, PABLO DANIEL, ALEXAKIS, A & POUQUET, A 2008 Nonlocal interactions in hydrodynamic turbulence at high reynolds numbers: The slow emergence of scaling laws. *Phys. Rev. E* **77** (3), 036306.
- NATRAJAN, V. K. & CHRISTENSEN, K. T. 2006 The role of coherent structures in subgrid-scale energy transfer within the log layer of wall turbulence. *Phys. Fluids* **18** (6).
- OBUKHOV, AM 1941 On the distribution of energy in the spectrum of turbulent flow. *Bull. Acad. Sci. USSR, Geog. Geophys.* **5**, 453–466.
- PAUL, I, PAPADAKIS, G & VASSILICOS, JC 2017 Genesis and evolution of velocity gradients in near-field spatially developing turbulence. *J. Fluid Mech.* **815**, 295–332.
- PIOMELLI, U., CABOT, W. H., MOIN, P. & LEE, S. 1991 Subgrid-scale backscatter in turbulent and transitional flows. *Phys. Fluids* **3** (7), 1766–1771.
- RICHARDSON, L.F. 1922 *Weather Prediction by Numerical Process*. Cambridge University Press.
- RICHARDSON, LEWIS FRY 1920 The supply of energy from and to atmospheric eddies. *Proc. Roy. Soc. London. Ser. A* **97** (686), 354–373.
- SAGAUT, PIERRE & CAMBON, CLAUDE 2008 *Homogeneous turbulence dynamics*, , vol. 10. Springer.
- SIROVICH, L. & KARLSSON, S. 1997 Turbulent drag reduction by passive mechanisms. *Nature* **388**, 753 EP –.
- TAYLOR, GEOFFREY INGRAM 1938 Production and dissipation of vorticity in a turbulent fluid. *Proc. Roy. Soc. London. Ser. A* **164** (916), 15–23.
- TAYLOR, GEOFFREY INGRAM & GREEN, ALBERT EDWARD 1937 Mechanism of the production of small eddies from large ones. *Proc. Roy. Soc. London. Ser. A* **158** (895), 499–521.
- TENNEKES, HENDRIK, LUMLEY, JOHN LEASK, LUMLEY, JONH L & OTHERS 1972 *A first course in turbulence*. MIT press.
- TSINOBER, ARKADY 2009 *An informal conceptual introduction to turbulence*. Springer.
- VELA-MARTÍN, ALBERTO & JIMÉNEZ, JAVIER 2021 Entropy, irreversibility and cascades in the inertial range of isotropic turbulence. *J. Fluid Mech.* **915**, A36.
- VEYNANTE, DENIS & VERVISCH, LUC 2002 Turbulent combustion modeling. *Prog. Energy Combust. Sci.* **28** (3), 193 – 266.
- YAO, JIE & HUSSAIN, FAZLE 2020 A physical model of turbulence cascade via vortex reconnection sequence and avalanche. *J. Fluid Mech.* **883**, A51.
- YOUNG, ROLAND M. B. & READ, PETER L. 2017 Forward and inverse kinetic energy cascades in jupiter’s turbulent weather layer. *Nat. Phys.* **13**, 1135 EP –.
- ZHOU, YE 1993*a* Degrees of locality of energy transfer in the inertial range. *Phys. Fluids* **5** (5), 1092–1094.
- ZHOU, YE 1993*b* Interacting scales and energy transfer in isotropic turbulence. *Phys. Fluids* **5** (10), 2511–2524.